TOROIDAL CONFIGURATIONS AS STABLE SOLITONS

L. Faddeev[*‡]   and   **Antti J. Niemi**[**‡]

[*]*St.Petersburg Branch of Steklov Mathematical Institute*
Russian Academy of Sciences, Fontanka 27 , St.Petersburg, Russia[‡]

[**]*Department of Theoretical Physics, Uppsala University*
P.O. Box 803, S-75108, Uppsala, Sweden[‡]

and

[‡]*Helsinki Institute of Physics*
P.O. Box 9, FIN-00014 University of Helsinki, Finland

Previously we have proposed that in certain relativistic quantum field theories knotlike configurations may appear as stable solitons. Here we present a detailed investigation of the simplest knotted soliton, the torus-shaped unknot.

1 Introduction

Lord Kelvin was the first to suggest that knotlike configurations might be of fundamental importance. In [1] he proposed that atoms, which at the time were considered as elementary particles, could be viewed as knotted vortex tubes in ether. Subsequently he also conjectured [2], that (thin) vortex filaments that have the shape of torus knots [5], [6] should be stable.

Kelvin's theory of vortex atoms has long ago subsided. However, at the time it was taken seriously, and it led to an extensive study and classification of knots. In particular the results obtained by Tait [3] remain a classic contribution to mathematical knot theory. Recently Kelvin's idea that different elementary particles can be identified with topologically distinct knots has been advanced in particular by Jehle [4].

Since its inception, Kelvin's conjecture on the stability of torus knots has also attracted much interest. However, it seems that until very recently [7], the issue has not been even properly addressed. This is due to the exceedingly complex nature of dynamical models that describe stable knots.

In order to study the dynamics of knotlike configurations in a predictive manner, we need a Lagrangian field theory where knots can appear as solitons. But in such a theory the equations of motion are generically highly nonlinear, to the extent that an analytic approach is hopeless. Indeed, even the identification of a Lagrangian where stable knotlike solitons can be present, has until recently defied all attempts. With the recent, rapid advances in computers it appears that by combining topological and geometrical methods in quantum field theories with high performance computing, a first principles analysis of Kelvin's conjecture is finally a reality [7].

In addition of elementary particles (atoms), Kelvin was also interested in knotlike configurations in a hydrodynamical context. Today there are numerous additional scenarios, where dynamical knots can be important: Presently it is commonly accepted that fundamental interactions are described by string theories [8], with different elementary particles corresponding to the vibrational excitations of a primary string. Even though connections between modern string theory and knot theory do exist, for example the Chern-Simons action is related both to conformal field theories and knot invariants [9], the possibility of an intimate relationship *e.g.* at some nonperturbative level remains to

be investigated. But in a number of other physical scenarios the potential relevance of knotlike structures has already been established [5], [6]. For example in early universe cosmology cosmic strings are supposed to be responsible for structure formation. These strings are expected to decay *e.g.* via gravitational fluctuations, but the possibility that stable knotted strings might survive should have important consequences. Furthermore, in QCD one may expect that gluonic flux tubes that confine quarks in hadrons could become tangled, suggesting that in pure Yang-Mills theory closed knotted flux tubes appear as physical states. Stringy knotted vortices might also appear in a variety of condensed matter physics scenarios. For example in type-II superconductors magnetic fields are confined within the cores of vortex-like structures. Recent experiments with ^{3}He-A superfluids have also revealed interesting vortex structures that can be described by theoretical methods which are adopted from cosmic string models. The study of knot-like configurations is also highly important for chemical compounds such as polymers. Finally, the investigation of knots is rapidly becoming an important part of molecular biology, where entanglement of a DNA chain interferes with vital life processes of replication, transcription and recombination.

Until now knotlike configurations have been mainly studied using non-dynamical, phenomenological models [10]. One first introduces a one-dimensional, structureless string and distributes some charge along it. The configuration is then allowed to relax into an equilibrium shape. However, such an approach is not dynamical, there are inevitably several knot-specific *ad hoc* parameters that need to be determined by various means. For example, the length of each topologically distinct knot is an independent degree of freedom. The details of the charge distribution also introduces some arbitrariness that can be parametrized. As a consequence of such parameters that are specific for individual knot configurations, the ensuing models lack in their predictive power. There is a definite need for a first principles approach where different knots emerge dynamically, as solitons. One can then predict their properties in terms of fundamental quantities which are in no manner specific to a particular knotted structure but characteristics of the underlying physical environment.

The literature on solitons is enormous, and there are several extensive reviews [11]. Until now the activity has mainly concentrated on 1+1 dimensions with the notable exceptions of the 2+1 dimensional vortex and nonlinear σ-model solitons, and skyrmeons

2

and magnetic monopoles in 3+1 dimensions. These are all pointlike configurations, that can not be directly associated with knotted structures.

When a pointlike two dimensional soliton is embedded in three dimensions, it becomes a line vortex. Since the energy of a vortex is proportional to its length, for a finite energy the length must be finite. This is possible if the core forms a closed, knotted structure. In 1975 one of us [12] proposed that a torus-shaped closed vortex could be constructed in a definite dynamical model. The configuration suggested in [12] is constructed from a finite length line vortex, twisted once around its core before joining the ends. The twist ensures that the configuration is stable against shrinkage. As a knot it corresponds to the *unknot* which is the simplest possible knotlike configuration [5], [6]. By combining geometrical and topological methods with high performance computing, we recently verified [7] the existence of such a soliton in the model proposed in [12]. Furthermore, we also found definite evidence for the existence of a soliton in the shape of a trefoil, which is the simplest possible torus knot. This is a strong indication, that the model proposed in [12] realizes Kelvin's conjecture on the existence of stable torus knots.

In this article we shall present a detailed investigation of the torus-shaped unknot soliton in the model proposed in [12]. In the next section we describe this model in detail, and in section 3. we specify it for torus-shaped solitons. In section 4. we reformulate the equations of motion so that a numerical construction of the unknot soliton can be performed, and in section 5. we present results of a model numerical simulation.

2   A Hamiltonian with Localized Solitons

In [7] we have proposed that certain relativistic field theories may admit solitons with the topology of a generic torus knot. In particular, we argued that such solitons can be described in terms of a three component vector field $\mathbf{n}(\mathbf{x})$ with unit length $\mathbf{n} \cdot \mathbf{n} = 1$. The action is [12]

$$S = \int d^4x \left(\frac{1}{2e^2}(\partial_\mu \mathbf{n})^2 + \frac{1}{4g^2}(\mathbf{n} \cdot \partial_\mu \mathbf{n} \times \partial_\nu \mathbf{n})^2 \right) \tag{1}$$

3

where we choose $\mathbf{n}$ to be dimensionless so that e determines a length scale and g is a dimensionless coupling constant. This is the most general relativistically invariant action for $\mathbf{n}$ that involves second and fourth order derivative terms so that time derivates appear only quadratically. It can be viewed as a U(1) gauged version of the Skyrme model [11]. However, the dynamical content of these two models are quite different.

Since time derivatives in action (1) appear only quadratically, it admits a canonical interpretation with static Hamiltonian

$$H = E_2 + E_4 = \int d^3x \left(\frac{1}{2e^2}(\partial_i \mathbf{n})^2 + \frac{1}{4g^2}(\mathbf{n} \cdot \partial_i \mathbf{n} \times \partial_j \mathbf{n})^2 \right) \tag{2}$$

The first term E_2 coincides with the nonlinear O(3) σ-model action, known to admit stable solitons in two dimensions. But if we include the fourth order derivative term E_4, stable finite energy solitons are also possible in three dimensions. This is suggested by the Derrick scaling argument: If we set

$$\vec{\mathbf{x}} \rightarrow \rho \vec{\mathbf{x}} \tag{3}$$

we find for our Hamiltonian

$$H = E_2 + E_4 \xrightarrow{\rho} \rho E_2 + \frac{1}{\rho} E_4 \tag{4}$$

so that stable finite energy solitons may exist when E_4 is present. In particular, we conclude that such solutions obey the virial theorem

$$E_2 = E_4 \tag{5}$$

A soliton described by $\mathbf{n}(\mathbf{x})$ is a localized configuration in R^3, at spatial infinity $|\mathbf{x}| \rightarrow \infty$ the vector field $\mathbf{n}(\mathbf{x})$ approaches a constant vector $\mathbf{n}_0$. Hence we compactify R^3 into a three dimensional sphere S^3, and $\mathbf{n}(\mathbf{x})$ can be viewed as a mapping from the compactified $R^3 \sim S^3 \rightarrow S^2$. Such mappings fall into nontrivial homotopy classes $\pi_3(S^2) \simeq Z$ that can be characterized by the Hopf invariant [5], [6]. For this we introduce the closed two-form

$$F = (d\mathbf{n} \wedge d\mathbf{n}, \mathbf{n}) \tag{6}$$

on the target S^2. Since $H_2(S^3) = 0$ its preimage $F_\star$ on the base S^3 is exact,

$$F_\star = dA_\star \tag{7}$$

4

and the Hopf invariant Q_H coincides with the three dimensional Chern-Simons term,

$$Q_H = \frac{1}{4\pi^2} \int_{R^3} F \wedge A \tag{8}$$

The existence of stable solitons in (2) with a nontrivial Hopf invariant is then strongly suggested by the lower bound estimate

$$H \geq c \cdot |Q_H|^{\frac{3}{4}} \tag{9}$$

where c is a nonvanishing numerical constant [13], [14].

In the following we shall find it useful to introduce a unit four vector $\Phi_\mu(\mathbf{x}) : R^3 \sim S^3 \rightarrow S^3$ and define two complex variables

$$Z_1(\mathbf{x}) = \Phi_1(\mathbf{x}) + i\Phi_2(\mathbf{x})$$
$$Z_2(\mathbf{x}) = \Phi_3(\mathbf{x}) + i\Phi_4(\mathbf{x})$$

so that

$$|Z_1|^2 + |Z_2|^2 = 1$$

and describe the unit three vector $\mathbf{n}(\mathbf{x})$ by

$$n^k = Z^\dagger \sigma^k Z \tag{10}$$

with σ^k the Pauli matrices. The two-form F_{ij} in (6) becomes

$$F_{ij} = i(\partial_i Z^\dagger \partial_j Z - \partial_j Z^\dagger \partial_i Z) \tag{11}$$

and modulo U(1) gauge transformations we have

$$A_i = \frac{i}{2}(Z^\dagger \partial_i Z - \partial_i Z^\dagger Z) \tag{12}$$

Under a local U(1) rotation $Z \rightarrow e^{i\gamma} Z$ both F_{ij} and $\mathbf{n}$ remain invariant while A_i suffers a gauge transformation $A_i \rightarrow A_i + \partial_i \gamma$. Hence Q_H is a functional of $\mathbf{n}$ only, and substituting in (8) we get

$$Q_H = \frac{1}{12\pi^2} \int d^3x \; \epsilon_{\mu\nu\rho\sigma} \Phi_\mu \; d\Phi_\nu \wedge d\Phi_\rho \wedge d\Phi_\sigma \tag{13}$$

which is the standard integral representation of the winding number for maps $S^3 \rightarrow S^3$, invariant under arbitrary local variations $\Phi_\mu \rightarrow \Phi_\mu + \delta\Phi_\mu$. In particular, (8) is an integer valued invariant of the vector field $\mathbf{n}(\mathbf{x})$.

3 Toroidal Solitons

In the following we shall be interested in the simplest possible knotlike soliton of (2), the torus-shaped unknot configuration [12], [14]. In this case we can introduce further simplifications using the fact that the Hamiltonian (2) is invariant under both spatial $SO(3)$ rotations and internal $SO(3)$ rotations of the vector $\mathbf{n}(\mathbf{x})$. Since we expect a torus shaped soliton to exhibit rotation invariance around its toroidal symmetry axis, this global $SO(3) \times SO(3)$ invariance will be broken into a diagonal $SO(2) \in SO(2) \times SO(2)$ invariance of combined spatial and internal rotations around the symmetry axis. Instead of minimizing the energy of the original Hamiltonian with respect to arbitrary variations of $\mathbf{n}(\mathbf{x})$, it is then sufficient to minimize the energy for the most general toroidal $SO(2)$ $\in SO(2) \times SO(2)$ invariant configuration $\mathbf{n}(\mathbf{x})$.

We select the toroidal symmetry axis so that it coincides with the z-axis in R^3, and align the asymptotic vector field $\mathbf{n}_0$ so that it points along the positive z-axis. In terms of cylindrical coordinates $(r, z, \psi) \equiv (\mathbf{y}, \psi)$, the most general Ansatz which is consistent with the toroidal $SO(2)$ symmetry then separates the angle ψ that describes rotations around the z-axis,

$$\mathbf{n}(\mathbf{y}, \psi) = \begin{pmatrix} \sin(\varphi(\mathbf{y}) + k\psi) \cdot \sin\theta(\mathbf{y}) \\ \cos(\varphi(\mathbf{y}) + k\psi) \cdot \sin\theta(\mathbf{y}) \\ \cos\theta(\mathbf{y}) \end{pmatrix} \tag{14}$$

Here k is an integer that counts the number of times the torus circles around the z-axis. Since (14) approaches the asymptotic constant vector $\mathbf{n}_0$ when $|\mathbf{x}| \to \infty$ and $\mathbf{n}_0$ points along the positive z-axis, we conclude that

$$\theta(\mathbf{y}) \overset{|\mathbf{y}| \to \infty}{\longrightarrow} 0 \quad mod \quad 2\pi \tag{15}$$

We substitute the Ansatz (14) in (2) and scale H appropriately by the dimensionless coupling constant g. In this way we find for the Hamiltonian

$$H = G^2 \cdot E_2 + E_4 = \int dr dz \; r \cdot \mathcal{E}(r, z)$$

$$= \int dr dz \; r \left(\frac{G^2}{4}(\theta_r^2 + \theta_z^2) + \sin^2\theta \cdot \left[\frac{G^2}{4}\left\{ \varphi_r^2 + \varphi_z^2 + \frac{k^2}{r^2} \right\} + \frac{1}{16}\left\{ (\varphi_r\theta_z - \varphi_z\theta_r)^2 + \frac{k^2}{r^2}(\theta_r^2 + \theta_z^2) \right\} \right] \right) \tag{16}$$

6

Here G is a dimensionfull coupling constant inversely proportional to length. Since there are no additional dimensionfull quantities, G specifies a length scale which determines both the size and the shape of the solitons. We note that H is invariant under $z \to -z$ reflections.

We introduce the following parametrization of the four-vector $\Phi(\mathbf{x})$,

$$\Phi = \begin{pmatrix} \cos\phi_{12} \sin\vartheta \\ \sin\phi_{12} \sin\vartheta \\ \cos\phi_{34} \cos\vartheta \\ \sin\phi_{34} \cos\vartheta \end{pmatrix} \tag{17}$$

From (10), (14) we then find

$$\begin{aligned} \varphi(\mathbf{y}) + k\psi &= \phi_{34} - \phi_{12} \\ \theta(\mathbf{y}) &= 2\vartheta \end{aligned} \tag{18}$$

For the gauge field (12)

$$A = \cos^2\vartheta \ d\phi_{34} + \sin^2\vartheta \ d\phi_{12} \tag{19}$$

and (6), (11) yields

$$F = dA = \sin 2\vartheta \ d\vartheta \wedge (d\phi_{34} - d\phi_{12}) \tag{20}$$

so that the Hopf invariant (8) becomes

$$Q_H = \frac{1}{\pi^2} \int \sin 2\vartheta \ d\vartheta \wedge d\phi_{34} \wedge d\phi_{12} \tag{21}$$

Here the expected local $S^1 \times S^2$ structure of our toroidal configuration is manifest.

From (16) we conclude that for a finite energy the angle $\theta = 2\vartheta$ must vanish on the z-axis,

$$\theta(r = 0, z) = 0 \quad mod \quad 2\pi \tag{22}$$

Together with (15) this implies that we can select $\theta = 0$ on the entire boundary of the half-plane (r, z). In order to have a nontrivial Hopf invariant we need that at some interior points (r_c, z_c) of the half plane we have $\theta(r_c, z_c) = \pi \quad mod \quad 2\pi$. For simplicity we assume that there is only one such point, and due to the $z \to -z$ symmetry of (16) we can select $z_c = 0$. This point determines the center of the toroidal configuration, a circle of radius r_c on the $z = 0$ plane of R^3 which is parametrized by the angle ψ.

In (17) the preimage of $\theta = 0$ corresponds to a circle which is parametrized by the angle ϕ_{34}. Similarly, the preimage of $\theta = \pi$ corresponds to a circle parametrized by the angle ϕ_{12}. Consequently we can refine (18) by the further identifications

$$
\begin{aligned}
\varphi(\mathbf{y}) &= \phi_{34} \\
k\psi &= -\phi_{12}
\end{aligned}
\tag{23}
$$

and for the Hopf invariant we obtain

$$
Q_H = \frac{k}{2\pi^2} \int \sin\theta \, d\theta \wedge d\varphi \wedge d\psi = \frac{k}{\pi} \int \sin\theta \, d\theta \wedge d\varphi
\tag{24}
$$

For a nontrivial Hopf invariant the angle $\varphi(\mathbf{y})$ must then increase (decrease) by 2π (more generally by $2\pi n$ with n an integer) when we go once around the center r_c on the (r, z) half plane. This means that the two circles parametrized by ϕ_{12} and ϕ_{34} corresponding to the preimages of $\theta = \pi$ and $\theta = 0$ respectively, are linked $(k \cdot n$ times).

Finally, if we assume that our toroidal soliton solution is an analytic function of the variables r and z, we conclude from (16) that its energy density vanishes at the center of the torus $\mathcal{E}(r_c, 0) = 0$, where θ has a maximum value $\theta = \pi$. Since the minimum value $\theta = 0$ occurs on the boundary of the (r, z) half plane, for an analytic soliton the energy density must also vanish there, and in particular along the z-axis. Hence $\mathcal{E}(r, z)$ must have a maximum value on a ring between the center r_c and the boundary of the half plane. This means that the energy density of a toroidal soliton is concentrated in a tube-like neighborhood around its center.

In the following we find it convenient to introduce stereographic coordinates $U(\mathbf{y})$, $V(\mathbf{y})$ on the (r, z) Riemann sphere, defined with respect to the north pole at $\theta = 0$

$$
\varphi = -\arctan\left(\frac{V}{U}\right)
\tag{25}
$$

$$
\theta = 2\arctan\sqrt{U^2 + V^2}
\tag{26}
$$

In these variables the Hamiltonian (16) becomes

$$
H = G^2 \cdot E_2 + E_4 = \int dr dz \, r \cdot \mathcal{E}(r, z)
$$

$$
= \int dr dz \, r \left\{ G^2 \left(\frac{U_r^2 + U_z^2 + V_r^2 + V_z^2}{(1 + U^2 + V^2)^2} \right) + \frac{k^2}{r^2} \frac{U^2 + V^2}{(1 + U^2 + V^2)^2} \right)
$$

8

$$+ \ \frac{(U_r V_z - U_z V_r)^2}{(1 + U^2 + V^2)^4} \ + \ \frac{k^2}{r^2} \frac{(UU_r + VV_r)^2 + (UU_z + VV_z)^2}{(1 + U^2 + V^2)^4} \bigg\} \tag{27}$$

and for the Hopf invariant we get

$$Q_H \ = \ -\frac{k}{\pi} \int \frac{dU \wedge dV}{(1 + U^2 + V^2)^2} \tag{28}$$

4   Flow Equation

The Euler-Lagrange equations for (16) are highly nonlinear and an analytic solution appears to be impossible. It seems to us, that the only tools available are numerical. However, even a numerical integration is quite nontrivial, there are several complications that need to be resolved. One concerns the (expected) chaotic nature of the equations of motion: We do not expect a direct Newton's iteration to converge towards a stable configuration unless we succeed in constructing an initial configuration which is very close to the actual solution. Rather, we expect Newton's iteration to exhibit chaotic behavior.

Due to lack of a proper initial configuration for Newton's iteration, we resort to alternative methods. For this we first formulate the problem at an abstract level, by considering a generic static energy functional $E(q)$ with some variables q_a. We introduce an auxiliary variable τ, and extend the (stationary) Euler-Lagrange equations of $E(q)$ to the following parabolic gradient flow equation

$$\frac{dq_a}{d\tau} \ = \ -\frac{\delta E}{\delta q_a} \tag{29}$$

Since

$$\frac{\partial E}{\partial \tau} \ = \ -\Big(\frac{\delta E}{\delta q_a}\Big)^2 \tag{30}$$

the energy decreases along the trajectories of (29). Furthermore, by squaring (29) and integrating from some initial value $\tau = T$ to $\tau \to \infty$ we get

$$\int\limits_T^\infty d\tau \Big(\frac{dq_a}{d\tau}\Big)^2 \ = \ \int\limits_T^\infty d\tau \Big(\frac{\delta E}{\delta q_a}\Big)^2 \tag{31}$$

9

Hence τ-bounded trajectories of (29) flow towards a stable critical point of $E(q)$. In particular, if we start at initial time $\tau = T$ from an initial configuration $q = q_0$ and follow a bounded trajectory of (29), in the $\tau \gg T$ limit we eventually flow to a stable critical point of $E(q)$

In (27) the fields $U(\mathbf{y})$, $V(\mathbf{y})$ correspond to the variables q_a, and by denoting $W_1 = U$, $W_2 = V$ the flow equation becomes

$$\frac{\partial W_a(\mathbf{y})}{\partial \tau} = -G^2 \cdot \frac{\delta E_2}{\delta W_a(\mathbf{y})} - \frac{\delta E_4}{\delta W_a(\mathbf{y})} \tag{32}$$

If we introduce the scaling (3) we find for the scaled Hamiltonian the flow equation

$$\frac{\partial W_a(\mathbf{y})}{\partial (\frac{1}{\rho}\tau)} = -(\rho^2 G) \cdot \frac{\delta E_2}{\delta W_a(\mathbf{y})} - \frac{\delta E_4}{\delta W_a(\mathbf{y})} \tag{33}$$

Thus a flow towards a toroidal soliton with coupling constant G coincides with the flow towards a toroidal soliton with coupling constant $\rho^2 G$, provided we rescale the flow variable τ into $\frac{1}{\rho}\tau$. This means that the soliton is essentially unique; It is sufficient to consider the flow towards a soliton with a definite value for G, since solitons with other values of G are obtained from this configuration by a simple scale transformation. Notice however, that in practice we perform a numerical integration of (32) on a finite lattice, and there are finite size corrections to the simple scaling (33).

An additional problem in a numerical approach is the selection of an optimal size for the lattice. If the lattice is too small in comparison to the scale that describes the soliton, the soliton may not fit into it. On the other hand, if the lattice is too large in comparison to the soliton, we may either miss the soliton entirely or use an unnecessarily large amount of computer time in constructing it.

The coupling constant G in (27) is the sole dimensionfull quantity that appears in our equations. Consequently it determines how both the location r_c of the center and the thickness of the soliton scale. Besides G, there are also dimensionless numerical factors that affect the overall size of the soliton. Since these numerical factors can only be obtained by actually solving the equations of motion, there are no *a priori* methods in selecting an optimal size of a lattice.

In order to approach these problems, we have developed a simple renormalization procedure that allows us to select the initial configuration so that the location r_c of its

10

center coincides with the location of the center for the actual soliton. For this we first observe that the soliton obeys the virial theorem (5), in our present variables

$$G^2 E_2 = E_4$$

By demanding that this virial theorem is also obeyed during the flow (32), we promote the coupling constant G into a τ-dependent variable $G \to G(\tau)$,

$$G(\tau) = \sqrt{\frac{E_4(\tau)}{E_2(\tau)}}$$

When we approach a soliton as $\tau \to \infty$, the variable $G(\tau)$ must then flow towards an asymptotic value G^* which is the value of the coupling for the soliton,

$$G(\tau) \overset{\tau \to \infty}{\to} G^* \tag{34}$$

This renormalization procedure fixes the location r_c of the center for the soliton, and allows us to choose the size of our lattice appropriately.

The thickness of the final soliton is also determined by the asymptotic value G^* of the coupling constant. However, since additional dimensionless numerical factors are also involved, the renormalization (34) does not help us in selecting the thickness of the initial condition so that numerical convergence is secured. This poses a problem for which we at the moment lack a firm solution, besides experimenting with various different types of initial configurations.

Finally, on a finite size lattice we also need to determine boundary conditions at the boundary of the lattice. On the (r, z) half plane the proper boundary condition for $U(r, z)$ and $V(r, z)$ is that both vanish on the boundary of the half plane. This corresponds to the compactification of the half plane into a Riemann sphere. However, we expect that on a finite lattice a simulation with such trivial boundary conditions leads to a flow towards the trivial configuration $U(r, z) \equiv V(r, z) \equiv 0$. In order to impose the boundary conditions properly in our numerical simulation, we have adapted an iterative process where we first specify the boundary conditions using the initial configuration $U_0(\mathbf{y})$, $V_0(\mathbf{y})$. At later values of τ we then update these boundary conditions successively, by interpolating the iterated configurations from the interior of the lattice to its boundary. In this manner we expect that we eventually obtain boundary conditions that correspond

11

to those of an actual toroidal soliton. An alternative method that we have used to determine the boundary conditions, is to start the iteration of (32) from a sufficiently large initial lattice with boundary conditions determined by the initial configuration. By successively shrinking the size of the lattice and determining boundary conditions in the shrinked lattice using the appropriate restriction of the pertinent iterated configuration from the larger lattice, we expect to converge towards boundary conditions that coincide with those of an actual soliton.

5   Numerical Simulation

We shall now present an example of a numerical construction of an unknot soliton. For simplicity we restrict to a configuration with Hopf invariant $Q_H = 1$ (*i.e.* $k = n = 1$), the other cases being treated similarly.

For a numerical integration of (32), we need an initial configuration with $Q_H = 1$ that properly approximates the final soliton. For this we introduce the standard complex bilinear transformation

$$\xi = \frac{\sigma - 1}{\sigma + 1} \tag{35}$$

and view it as a map between the unit disk $|\xi| \le 1$ and the $Re(\sigma) \ge 0$ half plane. By employing polar coordinates on the disk, we observe that the loci on the w-plane are circles, that at least in a qualitative sense coincide with our *a priori* expectations for the angular (25) and radial (26) behavior of a soliton (in coordinates where the center of a soliton coincides with $\theta = 0$).

Our soliton maps our compactified (r, z) half plane to a Riemann sphere. The variables $U(r, z)$ and $V(r, z)$ are stereographic coordinates with respect to the north pole $\theta = 0$, which topologically coincides with the entire boundary of the (r, z) half plane. As a consequence U and V determine a mapping from the (r, z) half plane to a disk, with the center of the disk at $\theta = 0$ (the entire boundary of the (r, z) half plane), while the rim of the disk is an (infinitesimally) small circle around the center of the soliton at $r = r_c$ where we have $\theta = \pi$. This suggests that we start our construction of an initial configuration by first setting

$$W(r, z) = U(r, z) + iV(r, z) = \frac{r + iz + \rho}{r + iz - r_c} \tag{36}$$

so that

$$
\begin{aligned}
U(r, z) &= 1 + (r_c + \rho) \cdot \frac{r - r_c}{(r - r_c)^2 + z^2} \\
V(r, z) &= -(r_c + \rho) \cdot \frac{z}{(r - r_c)^2 + z^2}
\end{aligned}
\tag{37}
$$

and the loci are circles on the U, V plane with

$$
(U - 1)^2 + (V + \frac{r_c + \rho}{2z})^2 = \frac{(r_c + \rho)^2}{4z^2}
$$

$$
(U - \frac{1}{2} - \frac{1}{2}\frac{r + \rho}{r - r_c})^2 + V^2 = \frac{1}{4}\frac{(r_c + \rho)^2}{(r - r_c)^2}
$$

Here $\rho > 0$ is a parameter, according to (35) the canonical value is $\rho = r_c$ but for the moment we leave it unspecified.

For (36) we have $\theta(r_c, 0) = \pi$ in (26). But in addition we need $\theta = 0$ on the entire boundary of the (r, z) half plane. For this we improve (36) into

$$
\begin{aligned}
U(r, z) &= F_U(r, z) \cdot \left(1 + (r_c + \rho) \cdot \frac{r - r_c}{(r - r_c)^2 + z^2} \right) \\
V(r, z) &= -F_V(r, z) \cdot \left((r_c + \rho) \cdot \frac{z}{(r - r_c)^2 + z^2} \right)
\end{aligned}
\tag{38}
$$

where F_U, F_V are appropriate positive valued functions, that vanish on the boundary of the (r, z) half-plane; For a proper initial configuration both F_U and F_V vanish sufficiently rapidly when we move away from the center at $r = r_c$, so that the initial configuration (in addition of the final soliton) can be fitted inside the lattice that we use in our simulation. We also need to specify these functions so that the Hopf invariant of the initial configuration coincides with the Hopf invariant of the desired soliton, in the present case $Q_H = 1$.

We have performed extensive numerical simulations for a soliton centered at $r_c = 6$, using several different initial profiles F_U and F_V, lattice structures and various alternative methods for ensuring independence from boundary behavior. Our simulations are consistently converging towards a definite toruslike configuration. As an example we now describe results from a particular simulation, based on the initial configuration (38)

with

$$F_U(r, z) = F_V(r, z) = b \cdot \frac{\exp(-d_1(r - r_c)^2 - d_2 z^2)}{c_1 + (r - r_c)^2 + c_2 z^2} \cdot (1 - \tanh[\sqrt{e_1(r - r_c)^2 + e_2 z^2}])$$
(39)

where $b, ..., e_2$ are parameters, fixed by minimizing the total energy (27) with respect to these parameters. This minimization is subject to the supplementary condition, that the overall size and shape of the initial configuration should resemble as much as possible the fixed point configurations that we have found in our earlier numerical simulations. In particular, we use the angular (φ) profiles of our earlier simulations to select an optimal value for the parameter ρ in (36).

In a simulation of the flow equation (32) we determine the length of each time step $\Delta \tau\_n = \tau_n - \tau_{n-1}$ adaptively, by demanding that the relative variation of total energy remains bounded,

$$|\frac{\Delta E(\tau_n)}{E(\tau_n)}| \leq 10^{-4}$$
(40)

We employ version 5.4 of the PDE2D finite element algorithm [15] using a sparse direct method with a 4th order Hermitean polynomial finite element basis. We have chosen a finite element approach, since it computes a continuous piecewise polynomial approximation to the solution. In a problem of topological nature this should be a definite advantage *e.g.* over a finite difference approach, where the solution is approximated only at discrete lattice nodes. In our example we have started from an initial square lattice with $0.001 \leq r \leq 14.0$ and $-6.0 \leq z \leq 6$, divided into a finite element mesh with 15.000 triangular elements. We have selected the triangulation so that it is more dense near $r \approx 0$ and $z \approx 0$, where we expect to have strongest dependence on the initial boundary conditions.

On the initial lattice we iterate the flow equation (32) until we reach a fixed point configuration described in figures 1a, 2a, 3a. We then introduce a sublattice with $0.1 \leq r \leq 13.5$ and $-5.5 \leq z \leq 5.5$, divided into a finite element mesh with 18.000 evenly distributed triangular elements. On this sublattice we determine both the initial and boundary conditions by restricting the previously obtained fixed point configuration to the sublattice. We then continue the iteration of the flow equation (32) until we again reach a fixed point, described in Figures 1b, 2b, 3b and 4-7.

In this two-phase simulation each of the phases takes about 200 hours of CPU time,

14

on a Digital Alpha Server 8400 equipped with EV56/440 MHz processors and 4GB of CPU. In the second phase with a larger number of triangles, our computation consumes about 725MB of CPU.

Our simulations reveal very strong convergence both for the coupling constant $G(\tau)$ and for the total energy $E(\tau)$ towards fixed point values; see figures 1-2. The length of the time step also increases exponentially when we approach the fixed point; see figure 3. Furthermore, we find very strong pointwise convergence for both of the angular functions $\theta(r, z)$ and $\varphi(r, z)$, and also for the density $Q_H(r, z)$ of the Hopf invariant; see figures 4-6. The integrated Hopf invariant Q_H is very stable under our entire simulation, essentially $Q_H \approx 1$ and for the final configuration we have $Q_H = 0.99997...$, when integrated over the final lattice.

Finally, for the energy density $\mathcal{E}(r, z)$ in (27) we have also found very strong pointwise convergence except in the vicinity of the origin $r \approx z \approx 0$. In this region we experience difficulties in fully eliminating the residual dependence of $\mathcal{E}(r, z)$ from our initial boundary condition along the z-axis. This slowness in pointwise convergence for very small r and z in $\mathcal{E}(r, z)$ can be related to our method: We use a finite element approach, where in each triangle of the mesh we approximate the solution by a 4th order Hermitean polynomial in r and z. Since $\mathcal{E}(r, z)$ involves r^{-2} terms, it is then conceivable that if the derivatives of $U(r, z)$ and $V(r, z)$ in (27) do not vanish sufficiently rapidly for small r, the pointwise convergence of $\mathcal{E}(r, z)$ may become slow in this region.

However, if we include the additional measure factor r in (27), it tames the r^{-2} behavior to the extent that the integrand of the total energy does exhibit very strong pointwise convergence. This is also the reason, why the difficulties we experience in eliminating the boundary dependence from $\mathcal{E}(r, z)$ as $r, z \to 0$ do not interfere with the overall convergence of the energy for our solution.

In figure 7 we present the energy density $\mathcal{E}(r, z)$ of our final configuration for $r \geq 0.3$, which is the region where we have confidence in the pointwise convergence of $\mathcal{E}(r, z)$ in the present example. The result is consistent with our qualitative picture: The energy density has a definite tubelike shape, essentially vanishing inside a tubular region around the center at $r = r_c$ and then attaining a maximum value in a surrounding collar-like region. At $z = 0$ the maximum value of the energy density is obtained for a relatively small value of $r = r_{max}$, and by combining results from a number of different simulations

15

we have arrived at an estimate that $r_{max} \leq 0.9$. For smaller values of r the energy density $\mathcal{E}(r, z = 0)$ then appears to decrease very rapidly, but due to the ensuing difficulties with small r convergence we can not verify that on the z-axis we actually have $\mathcal{E}(r = 0, z) \approx 0$. For this one needs to perform a high precision three dimensional simulation, such a simulation is now in progress and we plan to report on it in a future publication.

6 Conclusions

In conclusion, we have analyzed in detail the torus shaped unknot soliton using a high precision simulation. We have found very strong convergence towards a critical point of the energy, suggesting that we have indeed found a very good aproximation to an actual soliton. Our results indicate, that a combination of geometrical and topological tools in quantum field theory with high performance computing is finally making a first principles investigation of knotlike solitons realistic. In particular, our results indicate that Kelvin's conjecture on the existence of stable torus knots can be realized in the model that we have studied.

References

[1] W.H. Thomson, Trans. Royal Soc. Edinburgh **25** (1869) 217

[2] W.H. Thomson, in *Mathematical and Physical Papers IV* (Cambridge) (1911)

[3] P.G. Tait, *On Knots I II, III* Scientific Papers, Cambridge University Press, (Cambridge) (1898)

[4] H. Jehle, Phys. Rev. **D6** (1972) 441

[5] M. Atiyah, *The Geometry And Physics of Knots*, Cambridge University Press (Cambridge) (1990)

[6] L.H. Kauffman, *Knots And Physics*, World Scientific (Singapore) (1993)

[7] L.D. Faddeev and A.J. Niemi, Nature **387** (1997) 58

[8] M.B. Green, J.H. Schwarz and E. Witten, *Superstring Theory I, II* Cambridge University Press (Cambridge) (1987)

[9] E. Witten, Commun. Math. Phys. **121** (1989) 351

[10] J.K. Simon, Journ. Knot Theory and Raminif. **3** (1994) 299; D.W. Sumners, Notices of AMS **42** (1995) 528

[11] C. Rebbi and G. Soliani, *Solitons and Particles* World Scientific (Singapore) (1984); L.D. Faddeev and L.A. Takhtajan, *Hamiltonian Methods in the Theory of Solitons*, Springer-Verlag (Berlin) (1987)

[12] L.D. Faddeev, *Quantisation of Solitons*, preprint IAS Print-75-QS70 (1975); L.D. Faddeev, in *Einstein and Several Contemporary Tendencies in the Field Theory of Elementary Particles* in Relativity, Quanta and Cosmology vol. 1, M. Pantaleo and F. De Finis (eds.), Johnson Reprint (1979)

[13] A.F. Vakulenko and L.V. Kapitanski, Dokl. Akad. Nauk USSR **248** (1979) 810

[14] V.D. Makhankov, Y.P. Rybakov amd V.I. Sanyuk, *The Skyrme Model: Fundamentals, Methods, Applications* Springer-Verlag (Berlin) (1993)

[15] G. Sewell, Adv. Eng. Software **17** (1993) 105

Figure Caption

Figure 1a: Flow of coupling constant $G(\tau)$ towards its fixed point value G^*, for a soliton with $r_c = 6$.

Figure 1b: Flow of coupling constant $G(\tau)$ towards its fixed point value G^*, starting from the fixed point configuration described in Fig. 1a on a truncated sublattice, with boundary conditions also determined by the fixed point configuration in Fig. 1a. The slight difference in the fixed point values G^* after the first and second phase is partly due to a smaller and relatively more accurate lattice employed in the second run, and partly due to an improvement in the boundary conditions. Due to improved convergence there is also a $\mathcal{O}(10^3)$ increase in the final time step scales.

Figure 2a: Flow of total energy as a function of τ towards a fixed point. Notice that the energy decreases as a function of τ, as it should for a bounded trajectory.

Figure 2b: Flow of total energy as a function of τ towards a fixed point, starting from the fixed point configuration described in Fig. 2a on a truncated sublattice, with boundary conditions determined by the fixed point configuration in Fig. 2a. Notice that there is a $\mathcal{O}(10^3)$ improvement in the time step scales.

Figure 3a: Length of time step as a function of the number of iterations. The length of a time step is determined by the bound (40). The length should increase without a limit when a fixed point is approached.

Figure 3b: Length of time step for the second phase, starting from the configuration described in Figure 3b. The relative increase by a factor of $\mathcal{O}(10^3)$ from Fig. 3a can be attributed to improvements in boundary behavior and lattice accuracy.

Figure 4: The angle $\theta(r, z)$ for a fixed point configuration at the end of the second phase. Plotted on a sublattice with $0.3 \leq r \leq 12$ and $-4.5 \leq z \leq 4.5$. At the center $r_c = 6$ we have $\theta = \pi$, and outside of the soliton $\theta \approx 0$.

Figure 5: The angle $\varphi(r, z)$ for a fixed point configuration at the end of the second

19

phase. Plotted on a sublattice with $0.3 \leq r \leq 10$ and $-4.5 \leq z \leq 4.5$. When we go once around the center at $r_c = 6$, φ jumps by 2π. Notice the appearance of a tubular structure in the middle, corresponding to the interior of the soliton.

Figure 6: The density $Q_H(r, z)$ of the Hopf invariant, for the fixed point configuration at the end of the second phase. The tubular structure of a soliton is clearly visible. The integrated value of the Hopf invariant is very stable under our entire iteration, and for the final configuration we have $Q_H = 0.999997...$

Figure 7: The energy density $\mathcal{E}(r, z)$ for the fixed point configuration at the end of the second phase, plotted on a sublattice with $0.3 \leq r \leq 10$ and $-4.5 \leq z \leq 4.5$. The tubular structure is clearly visible, but near $r \approx z \approx 0$ we still have residual dependence on the initial boundary on the z-axis. This is understandable, since even a small error in the boundary condition can eventually give rise to a large local tension.
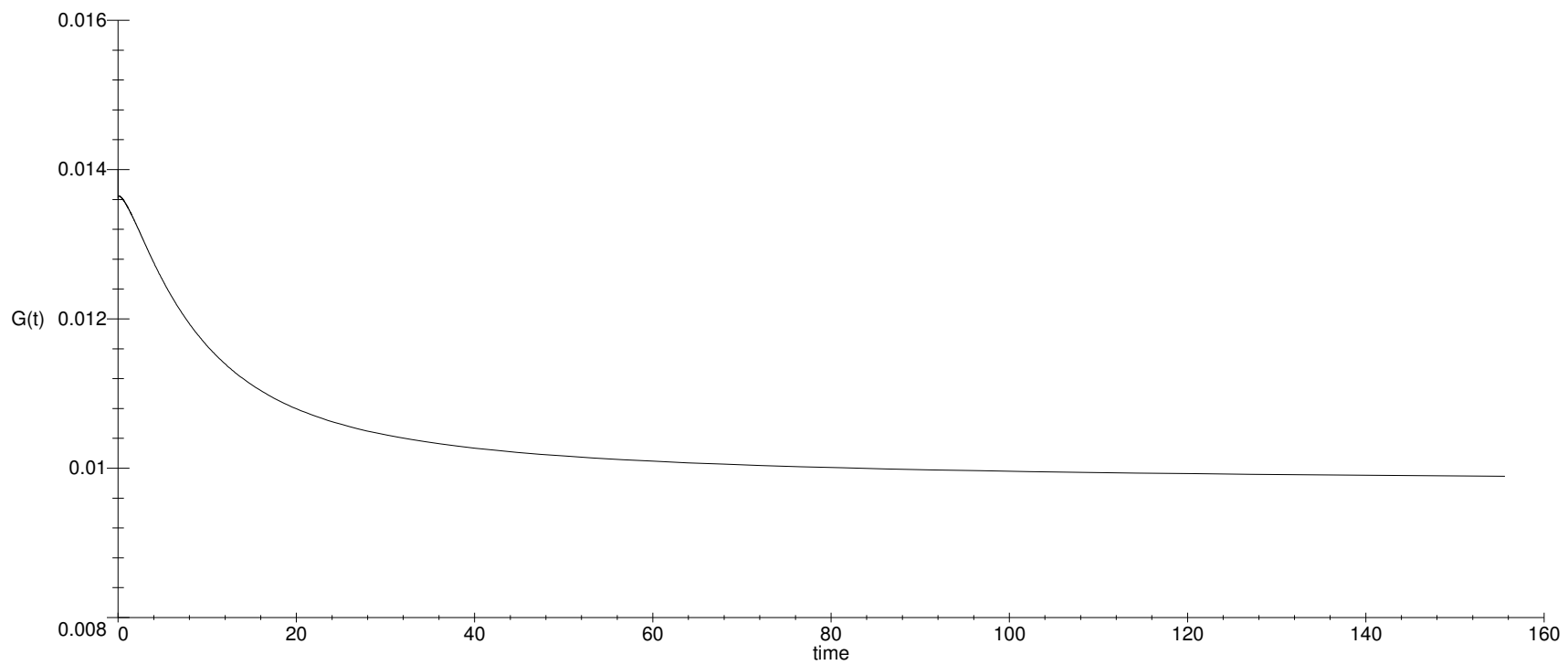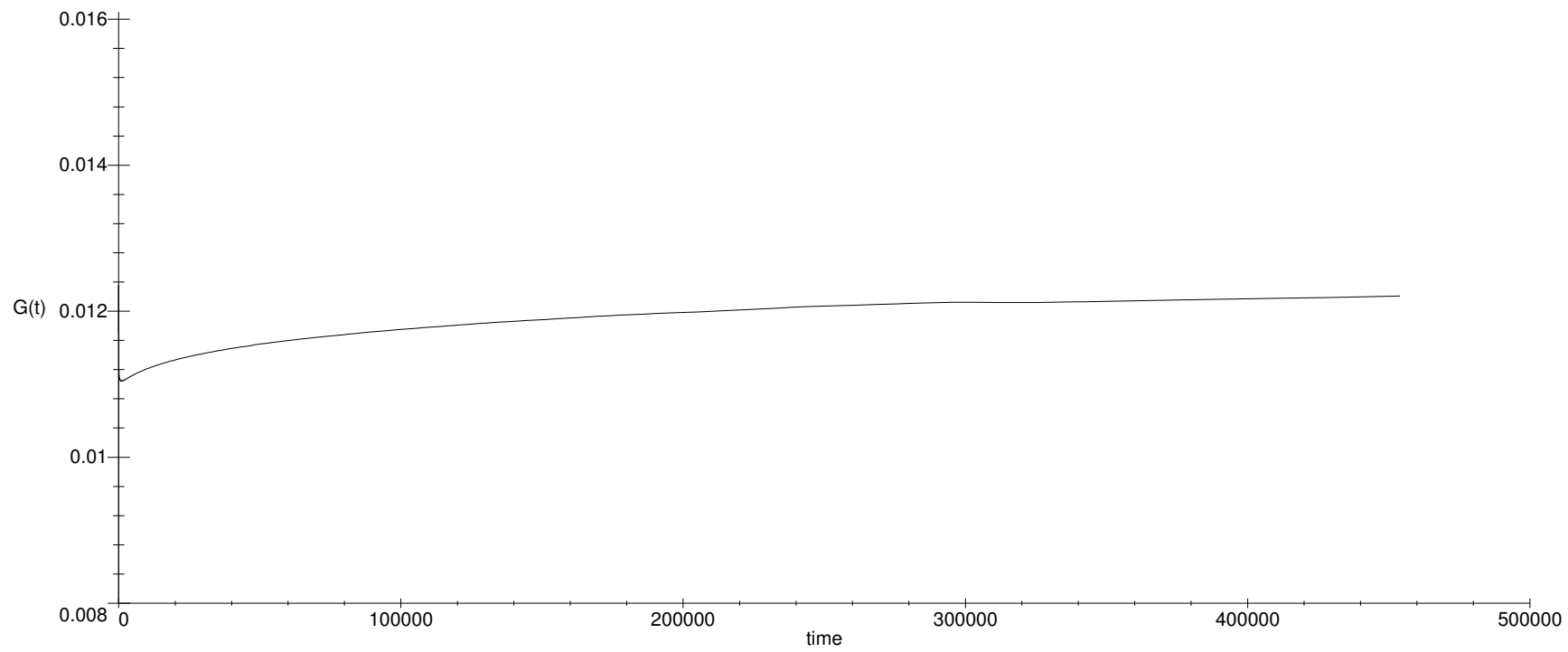
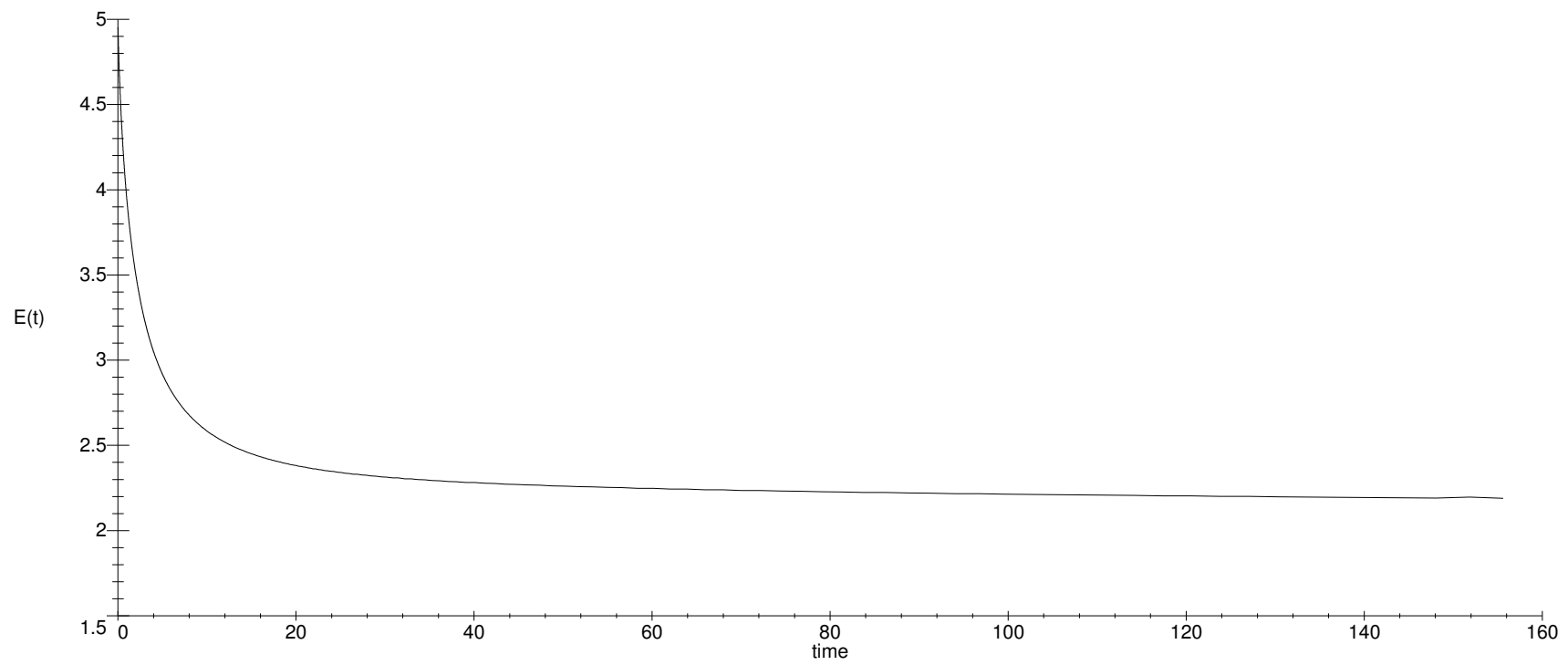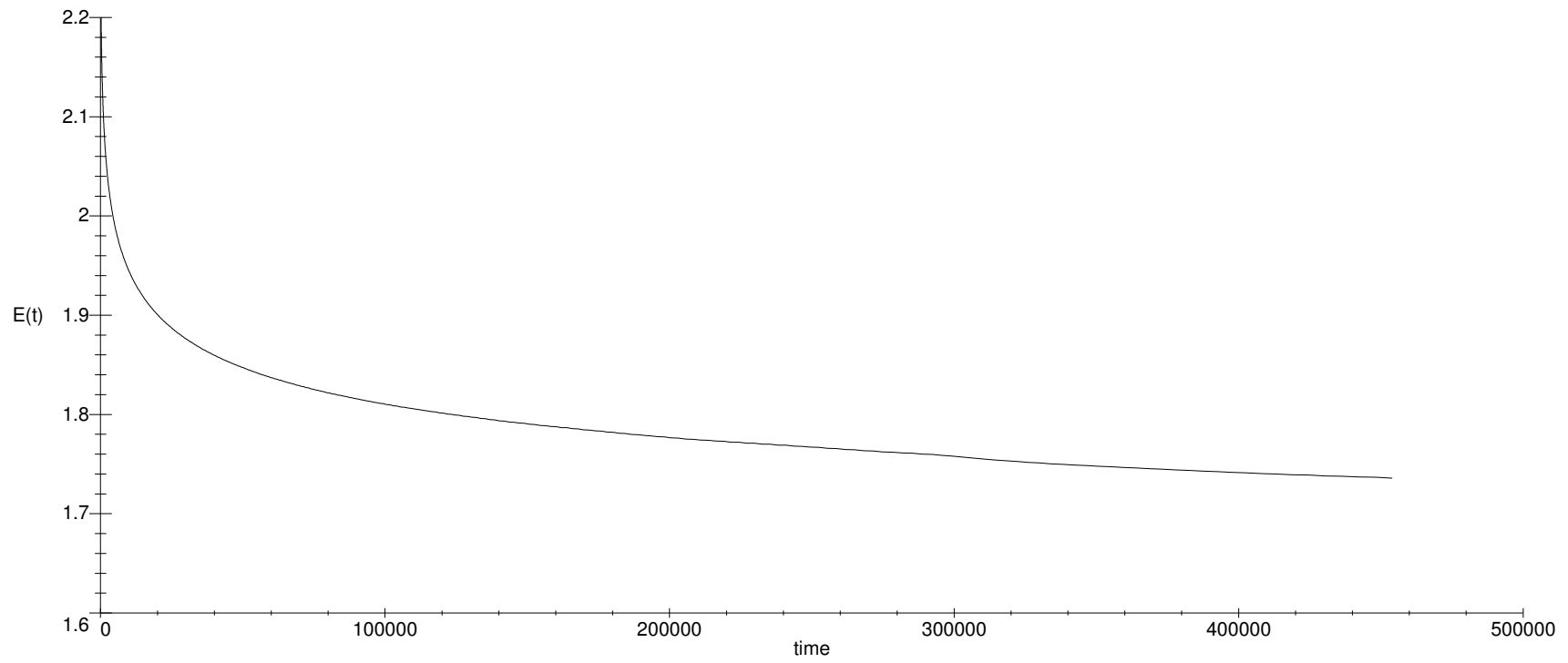Figure 1a

Figure 1b

Figure 2a

Figure 2b

Figure 3a

number of steps
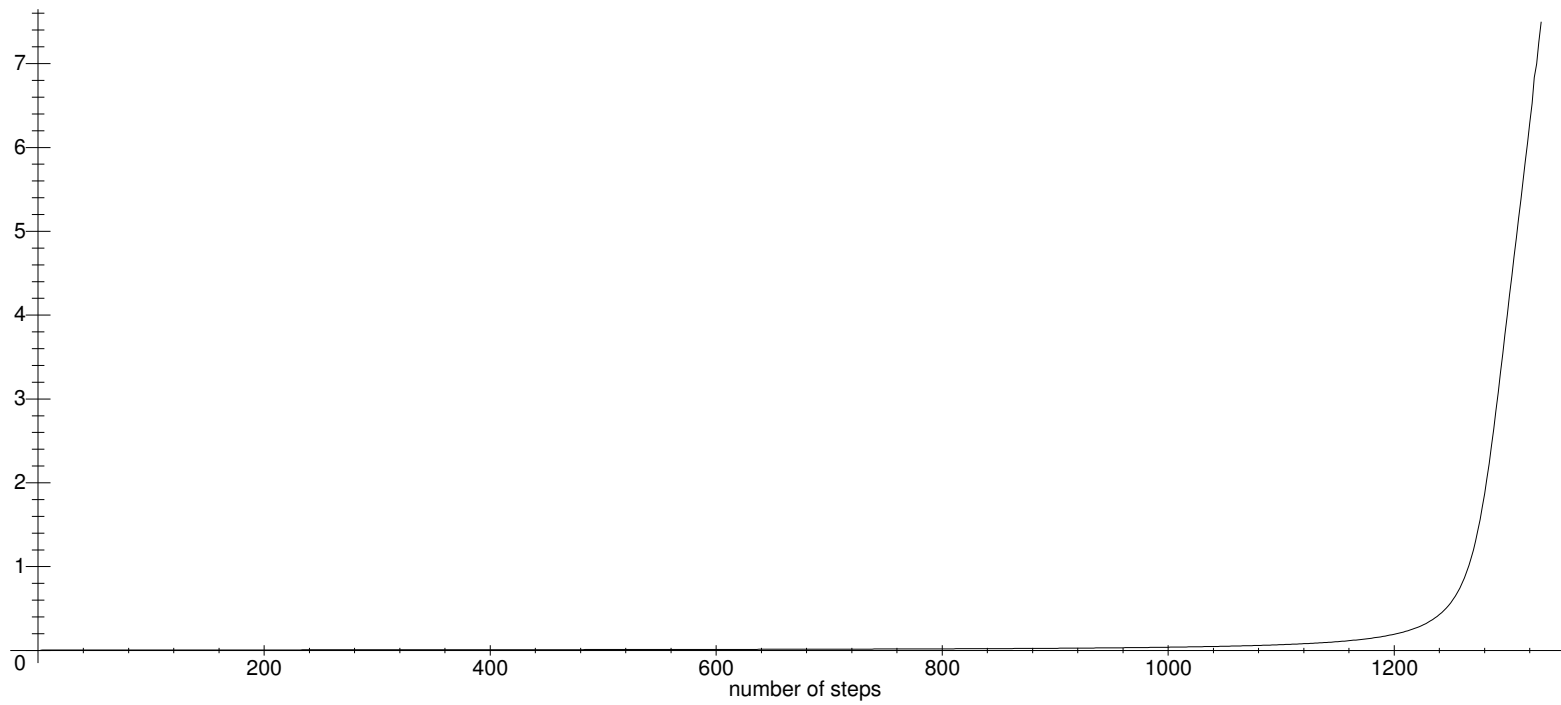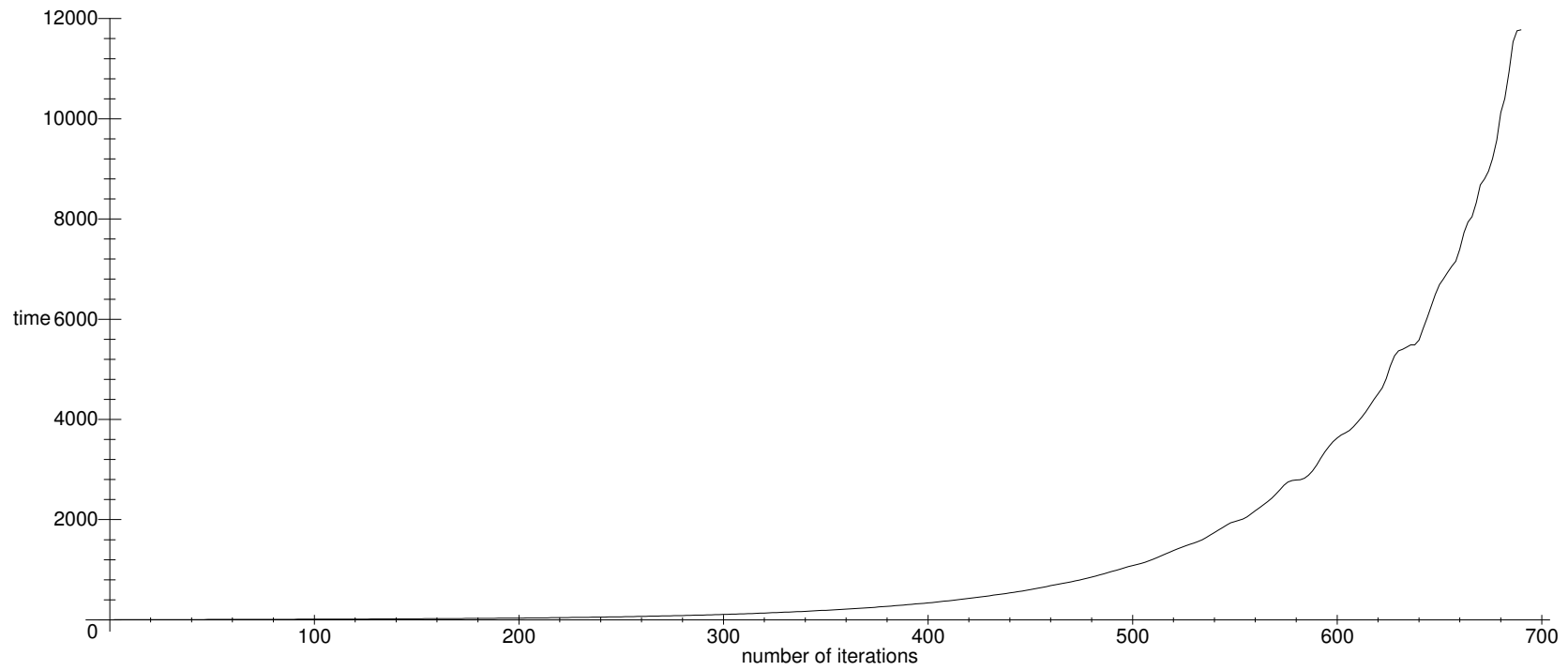
Figure 3b

This figure "figure4.gif" is available in "gif" format from:

http://arXiv.org/ps/hep-th/9705176v1

This figure "figure5.gif" is available in "gif" format from:

http://arXiv.org/ps/hep-th/9705176v1

This figure "figure6.gif" is available in "gif" format from:

http://arXiv.org/ps/hep-th/9705176v1

This figure "figure7.gif" is available in "gif" format from:

http://arXiv.org/ps/hep-th/9705176v1